

# Experimental Optics

**Contact person:**

Roland Ackermann

Friedrich-Schiller-Universität Jena

Abbe School of Photonics

Max-Wien-Platz 1

07743 Jena, Germany

Phone: +49 3641 9-47821, e-mail : [Roland.Ackermann@uni-jena.de](mailto:Roland.Ackermann@uni-jena.de)

**Last edition:** Roland Ackermann, February 2015

**Lab Title:** He-Ne Laser

<b>Group number</b>	G14
<b>Student name(s)</b>	Ke Li, Jerome Jahn
<b>Name of TA</b>	Ravil Idrisov
<b>Date of Lab</b>	March4,2019
<b>Date of Final Report return</b>	March7,2019

# Spectroscopy Laboratory Report

Ke Li, Jerome Jahn

March 2019

## Contents

<b>1</b>	<b>Introduction</b>	<b>3</b>
<b>2</b>	<b>Theory</b>	<b>3</b>
2.1	Helium Neon Laser . . . . .	3
2.2	Gaussian Beam, Stability Condition and the Resonator Modes . . . . .	4
2.3	Modes in a Laser Resonator . . . . .	5
2.4	Brewster's Angle and Laser Polarization . . . . .	6
2.4.1	Brewster Windows . . . . .	8
2.5	Transmission Grating . . . . .	10
2.6	Beam Parameter Product . . . . .	10
<b>3</b>	<b>Experimental Procedures</b>	<b>10</b>
3.1	General Setup . . . . .	10
3.2	Laser Alignment . . . . .	11
3.3	Measurement of Current vs Output Power . . . . .	12
3.4	Measurement of Cavity Length vs Output Power . . . . .	12
3.5	Measurement of Laser Tube Position vs Output Power . . . . .	12
3.6	Measurement of the Wavelength of Light . . . . .	12
3.7	Measurement of the beam quality factor $M^2$ . . . . .	13
<b>4</b>	<b>Results</b>	<b>13</b>
4.1	Beam Width and Stability of Different Resonators . . . . .	13
4.2	Relation Between Laser Output Power and Current Supply . . . . .	14
4.2.1	Setup M1:plane, M2: $R = 1000$ mm . . . . .	14
4.2.2	Setup M1: plane, M2: $R = 700$ mm . . . . .	16
4.3	Relation Between Laser Output Power and the Resonator Length	17
4.3.1	Setup M1:plane, M2: $R = 1000$ mm . . . . .	17
4.3.2	Setup M1: plane, M2: $R = 700$ mm . . . . .	19
4.4	Measurement of the Tube Position and Output Power . . . . .	21
4.5	Measurement of the Laser Wavelength . . . . .	22
4.6	Measurement of the beam quality factor $M^2$ . . . . .	22
4.7	Higher TME Mode . . . . .	24

<b>5</b>	<b>Discussion</b>	<b>25</b>
5.1	Injection Current and the Resultant Voltage across the Photodiode	25
5.2	Optical Cavity Length and the Laser Output Power . . . . .	27
5.3	Position of the Tube Laser in the Optical Cavity and Laser Out- put Power . . . . .	27
5.4	Determination of the Wavelength . . . . .	29
5.5	Laser Beam Quality Factor . . . . .	30
5.6	Suppressing the Fundamental Mode . . . . .	30
<b>6</b>	<b>Conclusion</b>	<b>30</b>
<b>7</b>	<b>References</b>	<b>31</b>

## 1 Introduction

This set of experiments explored various aspects of the He-Ne laser. In two different optical resonators the effect of the injection power on the laser output power and the effect of the cavity length on the output power was tested. Furthermore, the effect of the positioning of the lasing medium within a confocal cavity, the output wavelength of the laser, and the beam quality parameter within the beam product parameter was measured. Lastly, a higher order transversal mode was selected for through the use of a thin string suppressing the fundamental transversal mode.

The Helium-Neon gas laser is a very widespread laser emitting a variety of wavelengths. It is very prevalent in technology and science, having been used in devices from bar code scanners to alignment lasers for optical systems (1). They are relatively cheap lasers with a typical power source of electrons being accelerated between an anode and cathode.

## 2 Theory

### 2.1 Helium Neon Laser

Helium Neon laser is a laser system formed by a stable mirror cavity and a mixture of helium and neon gas with a ratio approximately between 5:1 and 20:1. Generally, a glass tube with helium and neon gas is placed in between the cavity, the gas in the tube is excited by the voltage applied to the anode and cathode of the glass tube, emitting a variety of wavelengths including one spectral peak of  $632nm$ . A diagram of the energy levels at play in generating emission wavelengths is shown in Figure 1.

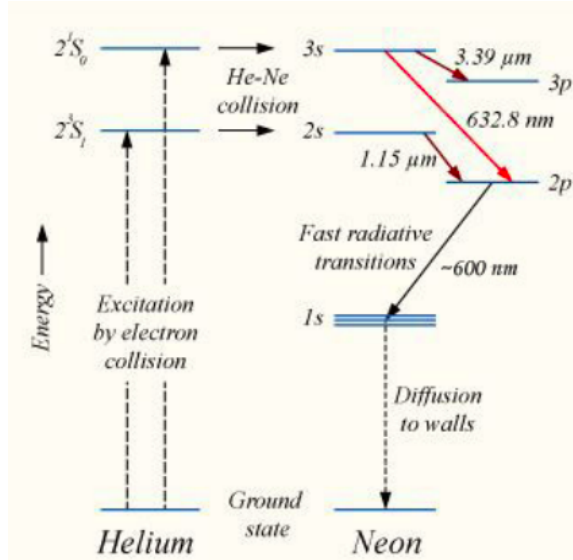


Figure 1: Four Level System of He-Ne Laser(2)

As shown above, helium atoms are excited by collisions with electrons being accelerated through the gas mixture from cathode to anode. The excited helium atoms collide with neon atoms in order to elevate them to the 3s level. These then decay to the 2p level and emit the wavelength 632.82. Natural broadening caused by Heisenberg uncertainty principle, collisional broadening, and Doppler broadening all are at play in giving the spectral peak at the named wavelength its lineshape. As the Doppler broadening dominates however, the main lineshape is of a Gaussian.

When the voltage between the anode and cathode is increased, the current increases, and the pump rate is increased. A larger population inversion is built up, and when the right wavelengths are able to resonate in an optical cavity, the stimulated emission causes a larger light amplification and thus output power.

## 2.2 Gaussian Beam, Stability Condition and the Resonator Modes

A laser beam is a coherent and collimated light beam whose intensity can be modeled by a Gaussian profile. The equation below shows the distribution of intensity of a Gaussian beam over space across an optical axis along z direction.

$$I(r, z) = I_0 e^{\frac{2r^2}{w(z)^2}} \quad (1)$$

where r is the radius of the Gaussian profile, and w(z) is the beam width of the Gaussian Profile,  $I_0$  is the initial intensity distribution of the Gaussian beam.

The beam width of such a Gaussian beam is defined as:

$$w(z) = w_0 \sqrt{1 + \left(\frac{\pi w_0^2}{\lambda z}\right)^2} \quad (2)$$

where  $\lambda$  is the central wavelength of the Gaussian or laser beam,  $w_0$  is the initial beam width.

To form a stable resonator of a Gaussian beam in a mirror cavity, meaning that the angle that a laser beam starting parallel to the optical axis makes with the optical axis does not increase as a function of the number of reflections, the radius of curvature of the wave front has to be equal to the curvature of the used resonators when the wavefront is incident on the respective mirrors. The stability parameters are defined as:

$$g_1 = 1 - \frac{d}{R_1}, g_2 = 1 - \frac{d}{R_2} \quad (3)$$

where  $d$  is the distance between the two mirrors that forms the lasing cavity, and  $R_1, R_2$  the radius of curvature of the two mirrors.

Considering the stability criterion mentioned above, the radius of the beam width can be written in terms of  $g_1, g_2$ :

$$w_0 = \left(\frac{\lambda d}{\pi}\right)^{\frac{1}{2}} \left[ \frac{g_1 g_2 (1 - g_1 g_2)}{g_1 + g_2 - 2g_1 g_2} \right]^{\frac{1}{4}} \quad (4)$$

From which we can derive the stability condition of a laser cavity in Eq. (5):

$$0 \leq g_1 g_2 \leq 1 \quad (5)$$

To observe a focused laser He-Ne laser beam along the central line of the laser cavity, it is important that the properties of the resonator meets the stability criterion. Laser from an unstable cavity suffers from high degree of diffraction after leaving the cavity, which are normally used in a very high gain, high-power condition instead of a laboratory study.(3)

### 2.3 Modes in a Laser Resonator

Electromagnetic waves propagation inside a medium are confined by the boundary conditions of electromagnetic waves, creating Transverse Electromagnetic Modes(TEM). In the He-Ne laser system, electromagnetic waves are cylindrically confined. This confinement leads to the generation of many TME modes of different order. Figure 2 is an image shows the shape and structure of TME modes that might be observed in the He-Ne laser system, where the first digit describes the number of radial zero fields, and the second digits describes the number of angular zero fields. Higher modes exist.

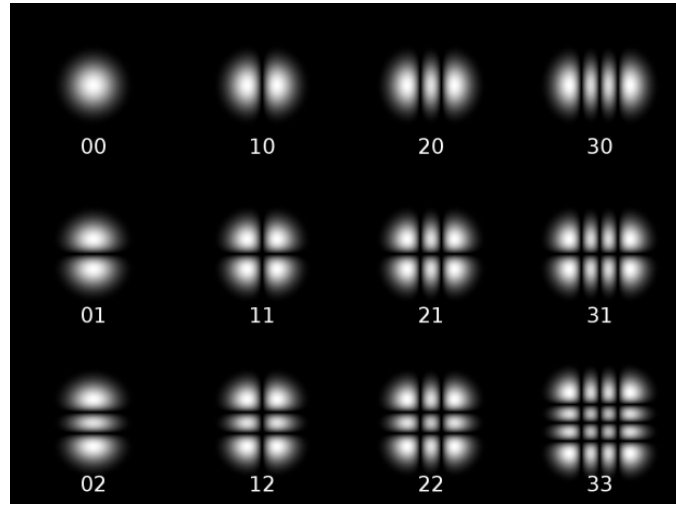


Figure 2: TME Modes in He-Ne Laser(2)

TEM are the solution Maxwell's Equation at the boundary of the cross section of the cavity. There are also longitudinal modes arising from the standing wave condition within an optical cavity. This condition described the possible oscillation frequencies that are able to build up in a laser cavity and fully experience the amplification effects stemming from the gain of the amplifying medium.

#### 2.4 Brewster's Angle and Laser Polarization

The interaction of a ray of light with a boundary between two isotropic media with different refractive indices results in a reflected and refracted component. The situation is depicted in Figure 3.

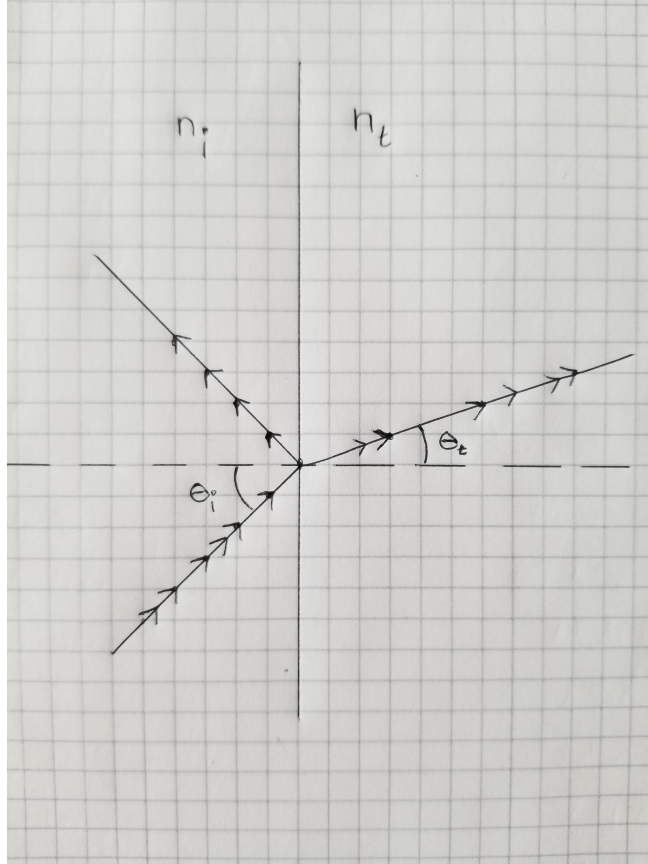


Figure 3: Interaction of Light with a Boundary between Two Isotropic Media With Different Refractive Indices

As is shown, the refractive medium of the light from which the light is hitting the surface is  $n_i$ , and the angle of incidence, measured from the normal to the surface, is  $\theta_i$ . The refractive index of the medium into which light is refracting is  $n_t$  and the angle of refraction, measured from the normal, is  $\theta_t$ . The quantitative relationship between these variables is described by Snell's Laws of Reflection and Refraction. The Law of Reflection is given in Eq. (6)

$$\theta_i = \theta_t, \quad (6)$$

and the Law of Refraction is written in Eq. (7)

$$n_i \sin \theta_i = n_t \sin \theta_t. \quad (7)$$

The coefficient of reflectivity  $R$  in this situation is usually defined as the ratio of the reflected intensity  $I_r$  to the incident intensity  $I_{inc}$  as shown in Eq. (8)

$$R = \frac{I_r}{I_{inc}}. \quad (8)$$

For what follows, a more useful concept is the amplitude reflectivity  $r$ , defined as the ratio of the reflected electric field wave amplitude  $E_r$  to the incident electric field amplitude  $E_{inc}$ , as shown in Eq. (9)

$$r = \frac{E_r}{E_{inc}}. \quad (9)$$

For homogeneous monochromatic plane waves, the relationship between the amplitude reflectivity and the intensity reflectivity is shown in Eq. (10)

$$R = r^2. \quad (10)$$

The component of the light parallel to the surface and the component perpendicular to the surface experience different reflectivities. The resulting relationship is encapsulated in Fresnel's equations for the reflectivity of the perpendicular and parallel incident amplitude components, written in Eq. (11)

$$r_{\perp} = \frac{n_i \cos \theta_i - n_t \cos \theta_t}{n_i \cos \theta_i + n_t \cos \theta_t}, \quad (11)$$

and Eq. (12)

$$r_{\parallel} = \frac{n_t \cos \theta_i - n_i \cos \theta_t}{n_i \cos \theta_i + n_t \cos \theta_t}. \quad (12)$$

In these equations,  $r_{\perp}$  and  $r_{\parallel}$  are the reflectivities of the electric field amplitude perpendicular to the surface and parallel to the surface, respectively. Upon analysis of these two equations, it can be seen that at  $\theta_i = 0^\circ$  (as in this case by Eq. (7)  $\theta_t = 0^\circ$  as well), the amplitude reflectivities of the parallel and perpendicular amplitude components will be equal to each other, albeit with a phase shift of  $180^\circ$  between them. At  $\theta_i = 90^\circ$ , the law cannot be used, and on the way to this extreme, both values again converge. At both of these extremes, by Eq. (10), their intensities are exactly equal to each other. In between this range, their values split. Interestingly, in Eq. (11), there can be found a value for which  $r_{\perp}$  reaches a value of 0. At this angle, perpendicular component of the incident light is transmitted fully, and only the parallel component experiences a reflectivity. This angle is dubbed the Brewster angle, and when light hits a surface at the Brewster angle the reflected light will be polarized in the plane of the surface of the light, whereas the refracted light will carry with it all of the perpendicular component mixed with the residual parallel component.

#### 2.4.1 Brewster Windows

This concept can be exploited in a Helium-Neon laser in order to have partially polarized light exiting the laser cavity. When the light exiting either side of the laser is incident at the Brewster angle on a slab of a transparent material, the

light will be mostly polarized in the plane of incidence as it is exiting the laser. There are two options for the orientation of the Brewster windows to each other, shown in Figures 4 and 5 below.

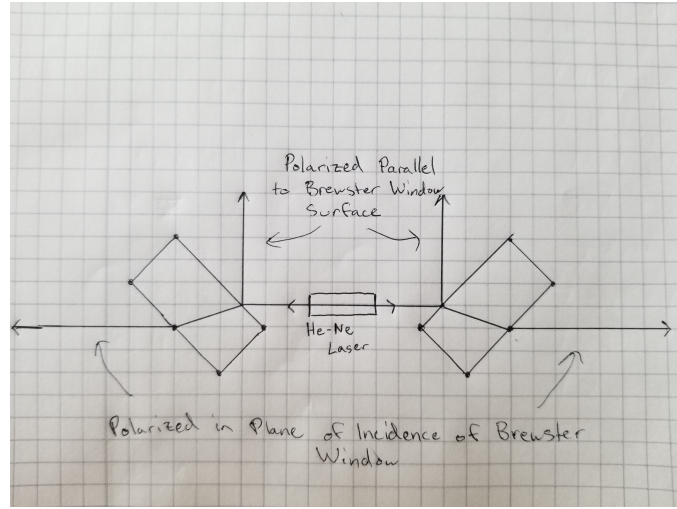


Figure 4: Possible Configuration of the Brewster Windows on either Side of a He-Ne Laser outputting light

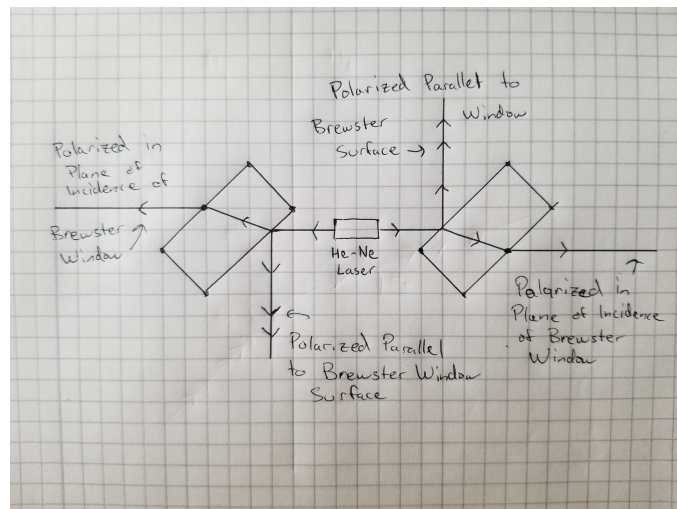


Figure 5: Possible Configuration of the Brewster Windows on either Side of a He-Ne Laser outputting light

The typical configuration that is chosen is the one shown in Figure 4, as there

would be no parallel shift difference in the light, and the emitted laser light from both sides does not need additional optics to be superimposed besides the optical resonator that would surround the laser cavity - brewster window combination.

## 2.5 Transmission Grating

A transmission grating is a series of periodically spaced slits. When the size of a slit is of the same order of the wavelength of the light trying to pass through it, diffraction can be observed. Diffraction is essentially an interference phenomenon between wavelets with their source at all points on the interior of the slit. The maxima, called the diffraction orders, of this interference pattern on an observation screen depend on the wavelength used. Thus, diffraction can be used to measure the wavelength of light. The effect of having a periodic arrangement of slits is that the maxima become sharper, allowing for more precise measurements. The formula for the angular positions of the maxima is given in Eq. (13)

$$g \sin \theta = m\lambda, \quad (13)$$

where  $g$  is the distance between the slits,  $\lambda$  is the wavelength of the light incident on the grating, and  $\theta$  is the angle formed between the position of the  $m$ th diffraction order and the 0th diffraction order, with the vertex of the angle lying in the center of the the point of intersection between the diffracting beam and the diffraction grating.

## 2.6 Beam Parameter Product

To exam and quantify the quality of our laser, the mathematical quantity BPP(Beam Parameter Product) could be used. The beam parameter product can be used to determine how good the beam can be focused to a small spot size.(2). It is mathematical expression in Eq. (14) below:

$$BPP = \theta w = M^2 \frac{\lambda}{\pi} \quad (14)$$

where  $w$  is the radius of the beam at its narrowest position,  $\theta$  is the angle of divergence of the beam,  $\lambda$  is the wavelength of the laser, and  $M^2$  is the beam quality factor, with a value possibly ranging from 1 to infinity. A beam quality factor of 1 indicates a beam with perfect Gaussian beam profile, while a beam quality factor larger than 1 indicates an imperfect Gaussian beam profile, due to higher modes or other factors in the laser system. (2)

# 3 Experimental Procedures

## 3.1 General Setup

In this experiment, we used the setup as shown in Figure 6.

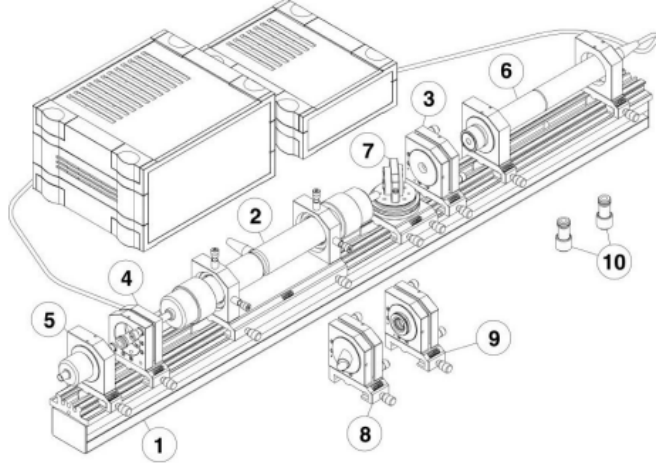


Figure 6: Experiment Setup(2)

As shown in the graph, 1 is the optical rail, (2) is the HeNe laser tube with power supply, 3 and 4 are laser mirror adjuster, 5 is photo detector in holder, 6 is alignment laser with power supply, 7 -8 are components not in use, 10 is a set of laser mirrors in holder.

The experiment used a longitudinal translation stage marked with a ruler on which the He-Ne gas laser medium together with pump source was mounted. The Brewster windows were already a part of this. Mounted around the gas laser medium were the mirrors constituting the optical cavity. On the left side, the spherical mirrors were placed. On the right side, a plane mirror that transmitted 2.4% of incident light was used. This light was led onto a photodiode. The voltage across the photodiode was amplified with a gain of 10 in order to be able to measure reliable values. The current in the gas lasing medium could be adjusted on the power source of the laser.

### 3.2 Laser Alignment

To align the laser system and obtain the optimal laser output, we first faced the side of the respective mirror that would later face towards the lasing medium toward the alignment laser beam and adjusted the mirror alignment until we observed that the alignment laser beam was reflected back to its emission spot. One sign of good alignment is when the reflected laser beam and the emitted laser beam produce an interference pattern. Another is when the intensity flickers. This symbolizes that the emitted alignment laser light is being reflected outside of the cavity and couple back into the alignment laser. This causes there to be other possible longitudinal modes able to resonate and steal the gain of the alignment laser, making the intensity of the red alignment laser flicker.

The alignment process was repeated for each mirror until a small red laser

spot was observed coming from the He-Ne gas tube. The alignment screws of the mirrors were then adjusted so as to give maximum output power. This alignment procedure was repeated every time that the geometry of the laser cavity was changed by changing the mirror positions on the rail. To increase the laser output, we also adjusted the alignment of the He-Ne tube so as to make the tube axis be coincident with the optical axis of the resonator. The mirrors were also periodically cleaned with an air pumping duster to get rid of any dust-induced mirror roughness.

### **3.3 Measurement of Current vs Output Power**

For two optical resonator cavities, the current running through the lasing medium was changed. One optical resonator cavity consisted of a mirror with radius of curvature being 100 cm and a plane mirror, and the other cavity consisted of a mirror with radius of curvature 70 cm and a plane mirror. In both optical cavities the mirror spacing was 50 cm. The current was taken from 5 mA to 6.5 mA in .1 mA steps and then decreased back down to 5 mA with .1 mA steps. The voltage across the photodiode was recorded at each step.

### **3.4 Measurement of Cavity Length vs Output Power**

The same two optical resonators were tested for the effect of changing the mirror spacing. For the optical resonator with the mirror with radius of curvature of 100 cm, the cavity length was taken from 50 cm to 84 cm in steps of 2 cm. For the other optical resonator, the cavity length was taken from 50 cm to 65 cm in steps of 1 cm. The photodiode voltage was recorded at each step.

### **3.5 Measurement of Laser Tube Position vs Output Power**

The mirror configuration of one mirror being spherical with radius of curvature of 100 cm and the other being planar was used with a mirror spacing of 50 cm. The laser tube was moved with steps of 1 cm from its edge closest to the plane mirror having a spacing from the inner edge of the plane mirror of 12 cm to 17 cm. The photodiode voltage was recorded at each of these positions.

### **3.6 Measurement of the Wavelength of Light**

First, the angle between the 0th and first diffraction order as found. This was done by projecting the diffraction orders on a wall perpendicular to the optical axis. This was done by measuring the distance between the diffraction grating and the wall, and then finding the distance on the wall between the 0th and first diffraction orders. The definition of the tangent function was used to infer the angle. The distance between slits was found from the label of the diffraction grating. Knowing the angle between the orders, the number of the order, and the separation between the slits, Eq. (13) was used to find the wavelength.

### 3.7 Measurement of the beam quality factor $M^2$

In this part of the experiment, we measured the beam quality factor  $M^2$  using a CCD camera and a convex lens. After aligning the laser, we focused the laser using a convex lens with a focal length of 150mm, observed the image captured by the CCD camera. To avoid over-exposure of the focused laser beam on the camera, we used a grey filter to reduce the over-exposed wavelengths and obtained a clearer images of the laser beam with sharper boundary. We recorded different images by moving the camera in 30 different positions. First, we captured 20 images with the camera moving 5 mm closer to the laser source each time, then captured 5 images with a 10 mm step size, lastly we captured another 5 images with a 5 mm step size.

From the images taken by the CCD camera, we used a Matlab program to find the center of gravity concerning gray values in captured images, made line scan in x-direction crossing the center of gravity, and fit a Gaussian distribution of the beams based on the images. The program also reconstructed the caustic of the beam and output result of the estimated  $M^2$ .

## 4 Results

### 4.1 Beam Width and Stability of Different Resonators

Different cavity properties give rise to different beam width and stability condition. Once we know the radius of curvature of the mirrors, we can calculate the stability parameters, and follow Equation (4) mentioned in the theory section, we can obtain the radius of the beam waist for different combination of mirrors. The calculation result of beam width of the four mirror combinations mentioned in the lab handout with a cavity length of  $d = 50\text{cm}$  is shown in Table 1.

Cavity	R of M1	R of M2	$w_0$ (mm)
Cavity 1	infinity	1000 mm	10.03 mm
Cavity 2	infinity	700 mm	7.98 mm
Cavity 3	infinity	infinity	Does Not Exist
Cavity 4	700 mm	1000 mm	8.4 mm

Table 1: Beam Width Calculation Result

In the table above, R stands for the radius of curvature of the mirror, M1, M2 stands for Mirror 1 and Mirror 2.

Using the stability criterion(equation 5) discussed in the theory section, we can plot the stability area of the four cavity combinations listed in the previous section. The calculation result is shown in the plots in Figure 7.

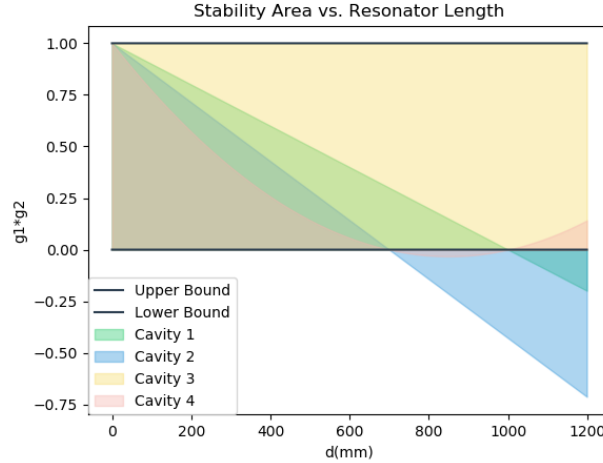


Figure 7: Stability Areas of Different Cavity

The stability ranges in terms of mirror spacing are also listed in Table 2.

Cavity Number	Stability Region
Cavity 1	$0 \text{ mm} \leq d \leq 1000 \text{ mm}$
Cavity 2	$0 \text{ mm} \leq d \leq 700 \text{ mm}$
Cavity 3	N/A
Cavity 4	$0 \text{ mm} \leq d \leq 700 \text{ mm}$ and $1000 \text{ mm} \leq d \leq 1700 \text{ mm}$

Table 2: Stability Regions of Optical Resonator Configurations

The planar mirror configuration stability condition implies that the spacing does not impact the stability. In reality, the stability of these mirrors depends on the angle of incidence and collimation of the light.

## 4.2 Relation Between Laser Output Power and Current Supply

In this part of the experiment , the gain of the power supply is set to 10 times, we adjusted the injection current from the lower limit (5mA) and increase the injection current to upper limit (6.5 mA) with a step of 0.1 mA, and repeated the measurement by decreasing the current back to the lower limit with the same step. The measurement results for the two different resonator setup is shown in the following sections.

### 4.2.1 Setup M1:plane, M2: $R = 1000 \text{ mm}$

The data is shown in Table 3.

Injection Current (mA)	Measurement 1(V)	Measurement2 (V)
6.5	$4.25 \pm 0.01$	$4.25 \pm 0.01$
6.4	$4.24 \pm 0.01$	$4.25 \pm 0.01$
6.3	$4.25 \pm 0.01$	$4.24 \pm 0.01$
6.2	$4.25 \pm 0.01$	$4.24 \pm 0.01$
6.1	$4.23 \pm 0.01$	$4.23 \pm 0.01$
6.0	$4.21 \pm 0.01$	$4.21 \pm 0.01$
5.9	$4.19 \pm 0.01$	$4.23 \pm 0.01$
5.8	$4.18 \pm 0.01$	$4.21 \pm 0.01$
5.7	$4.17 \pm 0.01$	$4.20 \pm 0.01$
5.6	$4.16 \pm 0.01$	$4.16 \pm 0.01$
5.5	$4.15 \pm 0.01$	$4.15 \pm 0.01$
5.4	$4.13 \pm 0.01$	$4.12 \pm 0.01$
5.3	$4.08 \pm 0.01$	$4.08 \pm 0.01$
5.2	$4.04 \pm 0.01$	$4.05 \pm 0.01$
5.1	$4.00 \pm 0.01$	$4.01 \pm 0.01$
5.0	$3.96 \pm 0.01$	$3.96 \pm 0.01$

Table 3: Injection Current vs. Output Power Result, R = 1000 mm

The uncertainty in the current reading  $C$  is gathered to be  $\Delta C = .05$ , stemming from the rounding of the machine. The data is plotted with uncertainty bounds in Figure 8.

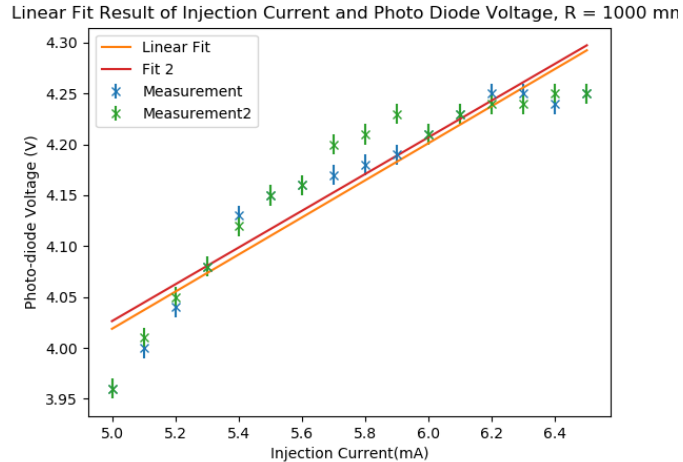


Figure 8: Injection Current VS Photodiode Voltage for Two Measurement

Nothing was changed about the experiment, and yet different values of the photo-diode voltage were obtained in the two data sets. The maximum difference in the measurements was measured at  $5.9 \pm .05$  mA, with a difference in

the two voltage measurements of  $.04 \pm .02$ . A direct relationship between the voltage on the photo-diode (and therefore the output power of the laser) and the injection current of the laser was found. The relationship was that the power of the laser increased along with the injection current. As described by our linear fit results as shown in Figure 8, the relationship could be coarsely mathematical formulated by a straight line. The slope of the linear fit of measurement 1 is:  $0.1825 \pm 0.009$ , the intercept is  $3.106 \pm 0.005$ , and the R value is: 0.946. The slope of the linear fit result of the second measurement is:  $0.1807 \pm 0.009$ , the intercept is:  $3.122 \pm 0.59$ , and the R value is: 0.931. Finally, we can conclude that our R values predict that the relation between injection current and output power is only coarsely linearly related.

#### 4.2.2 Setup M1: plane, M2: $R = 700$ mm

The data is shown in Table 4 below.

Injection Current (mA)	Measurement 1(V)	Measurement2 (V)
6.5	$7.56 \pm 0.01$	$7.50 \pm 0.01$
6.4	$7.56 \pm 0.01$	$7.51 \pm 0.01$
6.3	$7.54 \pm 0.01$	$7.50 \pm 0.01$
6.2	$7.52 \pm 0.01$	$7.49 \pm 0.01$
6.1	$7.51 \pm 0.01$	$7.47 \pm 0.01$
6.0	$7.48 \pm 0.01$	$7.45 \pm 0.01$
5.9	$7.46 \pm 0.01$	$7.43 \pm 0.01$
5.8	$7.44 \pm 0.01$	$7.45 \pm 0.01$
5.7	$7.40 \pm 0.01$	$7.42 \pm 0.01$
5.6	$7.36 \pm 0.01$	$7.38 \pm 0.01$
5.5	$7.34 \pm 0.01$	$7.32 \pm 0.01$
5.4	$7.29 \pm 0.01$	$7.28 \pm 0.01$
5.3	$7.24 \pm 0.01$	$7.24 \pm 0.01$
5.2	$7.19 \pm 0.01$	$7.18 \pm 0.01$
5.1	$7.13 \pm 0.01$	$7.13 \pm 0.01$
5.0	$7.06 \pm 0.01$	$7.07 \pm 0.01$

Table 4: Injection Current vs. Output Power Result,  $R = 700$  mm

The measurements were made after adjusting the alignment of the mirrors, cleaning the mirrors with a duster, and adjusting the orientation of the He-Ne tube to make sure it was parallel to the optical axis. These tweaks to the system greatly increased the voltage across the photo-diode. The uncertainty in the current readings was again taken to be  $\Delta C = .05$  from the rounding error of the machine. The two data sets with uncertainty bounds are plotted in Figure 9.

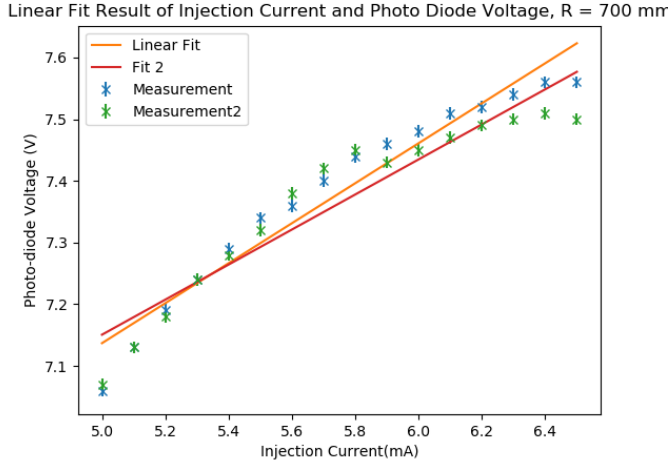


Figure 9: Injection Current VS Photo-diode Voltage for Two Measurement,  $R = 700$  mm

Once again, a direct relationship between the voltage on the photo-diode, and therefore the output power of the laser, and the injection current of the laser was found. While not perfectly linear, the relationship was that the power of the laser increased along with the injection current. Still, the relation might be coarsely modeled and understood by our linear fit result. The slope of the linear fit of the first measurement is:  $0.324 \pm 0.011$ , the intercept is:  $5.516 \pm 0.011$ , and the  $R$  value is: 0.972. The slope of the linear fit of the second measured is:  $0.284 \pm 0.11$ , the intercept is:  $5.730 \pm 0.0822$ , and the  $R$  value is: 0.944.

As for the reproducibility of the measurements, the two series were even more clearly different in this set. The maximum difference in the measurements was found to be when the injection current was at its maximum of  $6.5 \pm .05$  mA, with a difference between the voltage measurements of  $.06 \pm .02$ .

### 4.3 Relation Between Laser Output Power and the Resonator Length

#### 4.3.1 Setup M1:plane, M2: $R = 1000$ mm

In our first trial of measuring the relation between resonance length and the laser output voltage, we did not adjust the mirrors. With the roughness of the track and a potential misalignment of the axis of the He-Ne gas stage with the optical axis of the resonator, we found a sharp decrease in the output power. As stated, this was ascertained due to misalignment. The following measurements represent the maximum output power values when both mirrors were realigned.

The correct measurement data is shown in Table 5.

Cavity Length (cm)	Output Power (V)
50	5.60 ± 0.05
52	5.60 ± 0.05
54	5.67 ± 0.05
56	6.00 ± 0.05
58	5.78 ± 0.05
60	6.41 ± 0.05
62	6.73 ± 0.05
64	6.90 ± 0.05
66	7.05 ± 0.05
68	7.45 ± 0.05
70	8.12 ± 0.05
72	8.10 ± 0.05
74	8.06 ± 0.05
76	8.02 ± 0.05
78	8.06 ± 0.05
80	8.15 ± 0.05
82	8.26 ± 0.05
84	8.28 ± 0.05

Table 5: Resonance Distance and Laser Output Power, R = 1000 mm

As we can see from our measurement data, we can observe the general trend that the larger the resonance distance is, the higher is the voltage measured, the higher is the laser output power. The uncertainty in the measurement came from the flickering effect of the readings , and the amplification noise when the gain is set to above 1. Using a linear fit model, we can quantify the relation between resonance length and the laser output power. The scatter plot of our measurement data and the corresponding linear fit is shown in Figure 10.

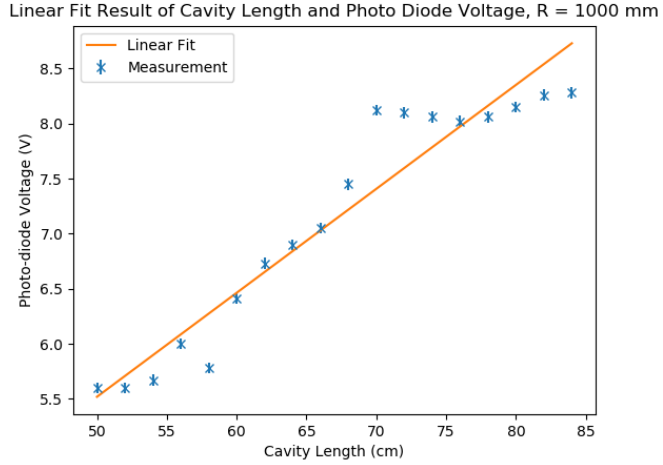


Figure 10: Scatter Plot and Linear Fit Result of Distance and Laser Output Power

As we can see from the scatter plot of our result, due to the uncertain performance of a gas laser, the output voltage does not show a perfect linear relation with the cavity distance. The slope of the linear fit result is:  $0.094 \pm 0.0016$ , the intercept is:  $0.798 \pm 0.0109$ , the R value is 0.958. Our R value suggests that the linear model describes 95.8% of the variability of our data points.

#### 4.3.2 Setup M1: plane, M2: $R = 700$ mm

Our measurement result of the cavity length and laser output power is recorded in Table 6.

Cavity Length (cm)	Output Power (V)
50	$7.57 \pm 0.03$
51	$7.75 \pm 0.03$
52	$7.55 \pm 0.03$
53	$7.56 \pm 0.03$
54	$7.63 \pm 0.03$
55	$7.41 \pm 0.03$
56	$6.88 \pm 0.03$
57	$6.22 \pm 0.03$
58	$6.16 \pm 0.03$
59	$6.18 \pm 0.03$
60	$6.03 \pm 0.03$
61	$5.62 \pm 0.03$
62	$4.9 \pm 0.03$
63	$3.72 \pm 0.03$
64	$2.22 \pm 0.03$
65	$0.88 \pm 0.03$

Table 6: Resonance Distance and Laser Output Power,  $R = 700$  mm

The uncertainty in the cavity length  $L$  measurement is taken to be  $\Delta L = .05$  cm, stemming from the smallest marks on the ruler attached to the optical setup. These values are plotted in Figure 11

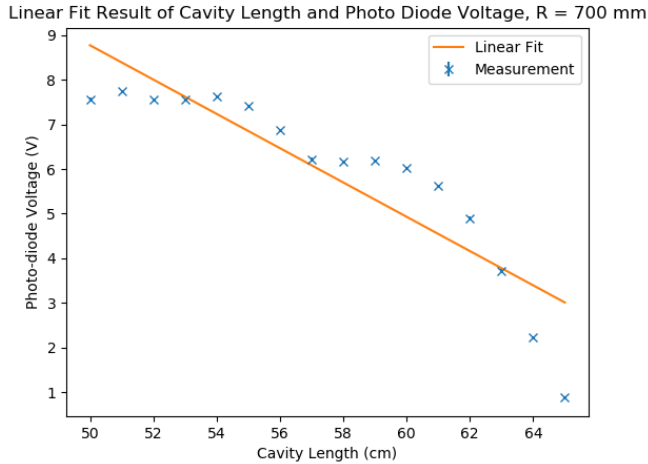


Figure 11: Cavity Length vs Photodiode Voltage for  $M_1$  having  $R = 700$  mm and  $M_2$  having  $R = \infty$

As cavity length increased, the output power decreased. For greater distances, a change in the distance had a greater impact on the output power. For

all the distances tried, the laser had a relatively stable output power with the uncertainties listed. This was expected, as the distance range was well within the bounds set by the stability condition in Eq. (5). Using a linear model, we might be able to quantify the change, the slope of the linear fit result is:  $-0.384 \pm 0.002$ , the intercept is:  $27.99 \pm 0.16$ , the R value is: 0.894. Our R value shows that the linear fit model only coarsely quantify the result, only covering 89.4% of the variability in our data points.

#### 4.4 Measurement of the Tube Position and Output Power

Using a plane mirror and a second mirror with a radius of curvature of 1000mm, we adjust the distance between the tube and the plane mirror from 12 cm to 17cm. Our measurement result is shown in Table 7.

Distance cm	Output Voltage (V)
$12 \pm 0.5$	$8.65 \pm 0.05$
$13 \pm 0.5$	$8.85 \pm 0.05$
$14 \pm 0.5$	$9.00 \pm 0.05$
$15 \pm 0.5$	$9.00 \pm 0.05$
$16 \pm 0.5$	$8.95 \pm 0.05$
$17 \pm 0.5$	$8.83 \pm 0.05$

Table 7: Tube Distance to Plane Mirror vs. Voltage Output

Plotting the data points and perform a linear fit algorithm, we can visualize the data as shown in Figure 12.

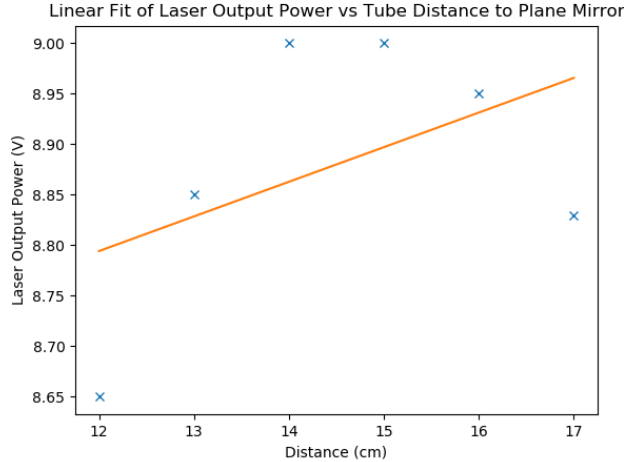


Figure 12: Tube Distance and Laser Output power

The slope of the fitted line is  $0.035 \pm 0.0075$ , the intercept of the fitted line is  $8.383 \pm 0.11$ , the p value of the linear fit is 0.3375, the R value is:0.478. As we can see, the data we collected do not strictly follow a linear relation.

#### 4.5 Measurement of the Laser Wavelength

The distance of the grating to the wall was measured as  $a = 168.6 \pm .1$  cm. The distance between the 0th and 1st diffraction order on the wall was measured to be  $o = 69.5 \pm .1$  cm. The definition of tangent is given in Eq. (15).

$$\tan \theta = \frac{o}{a} \quad (15)$$

Tangent is a nonlinear function. The value of  $\theta$  was found by considering the minimum and maximum values of the angle given the uncertainty. The minimum value of the angle is when  $o$  is at its minimum and  $a$  is at its maximum and found to equal  $\theta_{min} = 22.36^\circ$ . The maximum value of the angle is when  $o$  is at its maximum and  $a$  is at its minimum and found to equal  $\theta_{max} = 22.44^\circ$ . The value for the angle is then taken to be the  $\theta = 22.40^\circ \pm .04^\circ$ .

The diffraction grating had 600 slits per mm, and assuming that the size of the slits is tiny, dividing 1 mm by 600 gives the spacing between slits  $g = 1.67 * 10^{-6}$  meters.

The value of the wavelength is calculated from Eq. (13). As this involves a nonlinear function, the error propagation will be done by considering the maximum and minimum values the wavelength could have. The minimum value of the wavelength is when  $\theta$  is at a minimum and is calculated as  $\lambda_{min} = 635.3 * 10^{-9}$  meters. The maximum value is when  $\theta$  is at a maximum and is calculated as  $\lambda_{max} = 637.5 * 10^{-9}$  meters. The experimental value for the the wavelength is then  $\lambda = 636.4 * 10^{-9} \pm 1.1 * 10^{-9}$  meters.

#### 4.6 Measurement of the beam quality factor $M^2$

Using a Matlab program given, we extract the center of gravity concerning gray values in captured images, and fit a Gaussian distribution with parameters A, B, and C according to the formula below for each images:

$$G(x) = Ae^{-2\frac{(x-B)^2}{C}}. \quad (16)$$

The result output from the Matlab program of the Gaussian fit is shown in Figure 13:

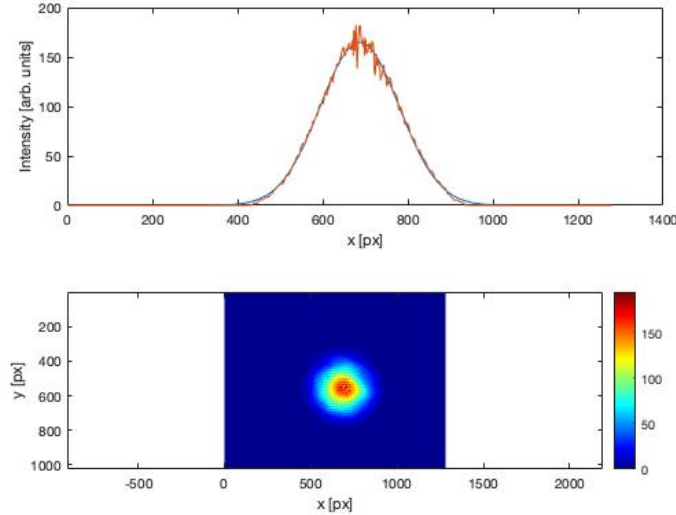


Figure 13: Gaussian Fit Result

As we can see from the figure, the images of the laser spot can be fitted by a Gaussian curve, with strongest intensity at it's central wavelength. From the fitted Gaussian parameter C, we can estimate the spot radius for every images. The result of the spot radius in both x and y direction calculated by the Matlab program is plotted shown shown in Figure 14.

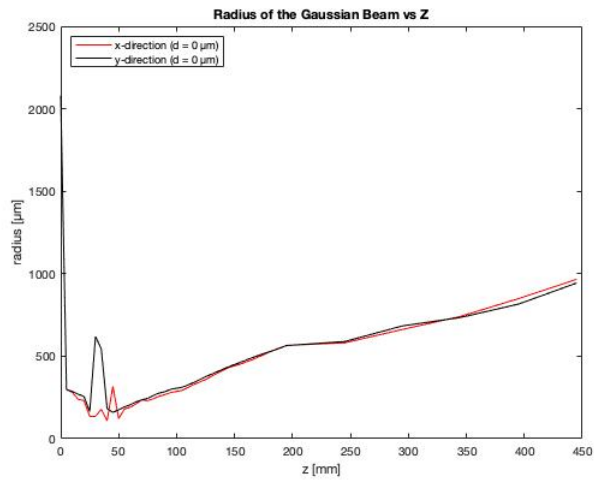


Figure 14: Spot Radius Calculation Result in both x and y Direction

From the radius of the spot, we can estimate and obtain the relation the beam width of the Gaussian beam and the distance of from the narrowest beam width, which can help us estimate the beam quality factor of the laser we setup in this experiment. The relation between beam width and the beam quality factor is shown in the equation below:

$$w^2(z) = w_0^2 + (M^2)^2 \left( \frac{\lambda}{\pi w_0} \right)^2 (z - z_0)^2 \quad (17)$$

where  $z_0$  is the location of the narrowest beam width, and  $w_0$  is the narrowest beam width.

The result output from the program of the caustic fit based is shown in Figure 15:

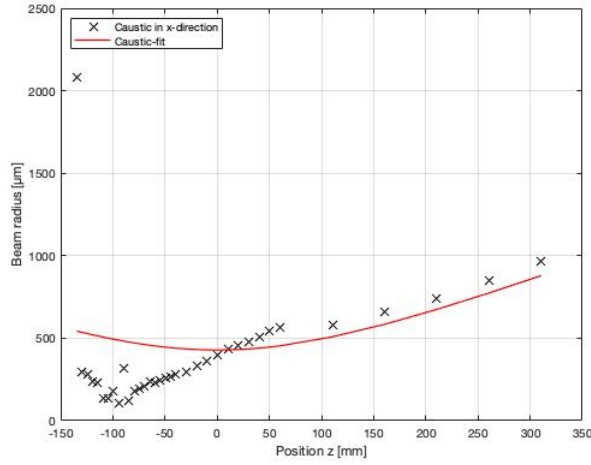


Figure 15: Caustic Fit Result

From the caustic fit result, the program estimated that the beam quality factor is:  $M^2 = 5.264$ . This value shows large deviation from the beam quality factor value of the fundamental mode of a typical He-Ne laser of 1.1 (4), indicating an imperfect beam quality.

#### 4.7 Higher TME Mode

By placing a thin filament inside the laser cavity, adjusted the filament to a suitable position, we obtained a second order Transverse Electromagnetic Mode, as shown in Figure

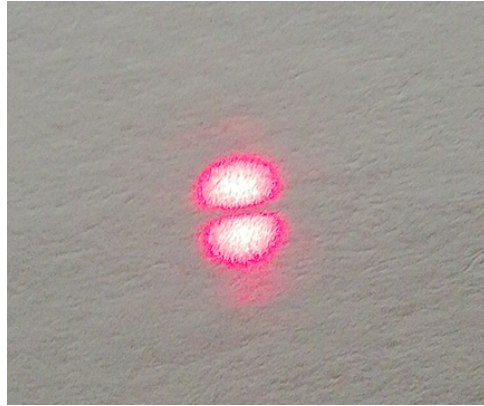


Figure 16: Higher TME Mode

As we can see, the thin filament placed in the cavity increased the loss of the laser output, so that the total energy of the laser beam was reduced, resulting in a higher order mode.

## 5 Discussion

### 5.1 Injection Current and the Resultant Voltage across the Photodiode

For both optical cavities, a hysteresis effect was seen in the voltage measurements. These results were very intriguing. The voltage on the photodiode in an integration time is proportional to the power of the light hitting the photodiode. The proportionality involves aspects of the setup that were not measured such as photocurrent in the photodiode and the efficiency of photodiode at turning incident light of a certain wavelength into photocurrent. Without knowledge of these aspects, the determination of the actual power of the laser is impossible. However, it can be said that when the voltage on the photodiode doubles, the power incident on the photodiode stemming from the laser also doubled.

The reason for stable output power of the He-Ne laser in cw operation is a continuous pump rate leading to a stable population inversion of which a portion is decaying through stimulated emission at a constant rate. If the lasing medium exhibits such perfect rates of transition, then with smooth mirrors reflecting light back into the lasing medium and perfectly constant indices of refraction in the passages of air that the laser pass through, this would lead the light to hit the photodiode at a constant rate. Besides thermal or amplification noise, stemming from dark noise in the photocurrent, the reading would be constant.

In actuality, the uncertainty in the voltage measurements was due to a very noticeable fluctuation of the photodiode voltage not due to thermal noise. It was not thermal noise as there was no fluctuation in the photodiode voltage value

when no laser light was incident on the photodiode. This implies a fluctuation of the output power of the laser. This could be due to changing mirror roughness and unclean air causing a constantly changing level of dust in the path of the beam, causing unpredictable phase shifts. Besides these reasons, it could also be indicative of the fact that there was not a constant power emitted by stimulated emission. This in turn indicates that there was not a perfect matching of the rate at which electrons are reaching the lasing energy level through spontaneous decay from higher energy levels to the rate of electrons leaving the lasing energy through stimulated emission. The reasons for such a mismatch are plentiful and have to do with the flow of energy in the lasing medium from the injection current to the lasing energy level. As can be seen in Figure 1, the path that the electrical energy takes to being the Neon electron's total energy in the 2p orbital is far from being straightforward. If the collisional energy transfer does not have a well-defined time average, or if this energy transfer fluctuates with a period similar to the sampling rate of the photodiode, then that would lead to the observed behavior. If this rate from perhaps an inconsistent rate of collisional energy transfer from the helium to the neon gas atoms, or perhaps a broadening of the . Even the heat of being too close to the setup causing minuscule thermal drafts could have impacted our readings.

A further consideration is that the injection current causes a magnetic field in the gas. If the injection current is not *perfectly* stable, then it would cause fluctuations in the magnetic field. A fluctuating magnetic field would cause a fluctuating electric field, which would seek to accelerate the electrons in the current. This would cause further fluctuations in the continuity of the current within the gas, and the cycle would repeat. As the current is being generated by an anode and cathode with a high voltage difference between them, and they are separated by gas, the current would be a function of the density and temperature of the gas. In general in gases, these are two variables which may only be constant when considering the average value within a volume constituting a closed energy system. It is safe to say then that there is some effect due to the fluctuations in the continuity of the current from the mechanism described above, although it is not known without further calculations and experiments the size of the effects and whether they impacted the measurements.

The complexities of tracing the source of error in the unstable, hysteretic output power of the Helium-Neon laser call for a multitude of experiments to determine the causes and dynamics at play. A host of experiments, each isolating any one of the variables mentioned above, would need to be performed. Performing the same measurements in a vacuum and comparing the behavior of the output power with the ones in this experiment could help understand whether air impurities and temperature are a significant source of error. The mirrors could be tested using a Fizeau interferometer to see whether the wave front of the light is changed an appreciable amount from the ideal spherical or planar shape expected in our cavity. The gas mixture inside could be altered in terms of composition, density, or temperature, to see whether variation in any of these variables are directly proportional to any kind of random fluctuations in output power. The current through the medium could be altered at a

variety of jumps to see whether the impacts of the current's feedback from the electromagnetic field interaction is a source of error. These experiments would be starting points to gain understanding of the Helium-Neon laser.

## 5.2 Optical Cavity Length and the Laser Output Power

The observed trend depended on the mirror configuration used. For the first configuration with a spherical mirror of radius 100 cm, the increase in distance led to an increase in the output power that was roughly linear. For the second configuration with a spherical mirror of radius 70 cm, the increase in distance led to a decrease in the output power that was also roughly linear.

This behavior is at first puzzling. It could be explained by the data evincing not a fundamental relationship being studied, but a serious misalignment of our lasing medium. It was not properly tested whether the lasing medium's axis was on top of the optical axis of the resonators. As the mirrors needed to be regularly realigned in order to maximize the output power, it is likely that this indeed was not the case, and that the intersection of the beams with the lasing medium was never maximized. In other words, the resonating frequencies in the optical cavity were never running parallel to the lasing medium. As the distance between the mirrors increased, the alignment of the mirrors that caused a maximum output power was always a very different one. In other words, only one mirror was moved, and yet two mirrors needed to be realigned. If the necessity of the realignment came from a shift in the orientation of the spherical mirror due to the roughness of the track, then only the spherical mirror should have had to have been realigned to reach the maximum output power. Instead, the planar mirror also always needed to be realigned. This implies that the optimal path for the ray through the misaligned lasing medium was a function of the cavity spacing. Hence, there was a systematic error introduced in all measurements where the mirror separation or the lasing medium was measured, and the light also cut a new path through the gain medium at each new configuration.

The expected result was that the output power decreased with mirror spacing. This comes from the fact that the further the plane mirror is from the focus of the other spherical mirror, the more reflections may not be coupled back into the gain medium.

## 5.3 Position of the Tube Laser in the Optical Cavity and Laser Output Power

The expected impact of the position of the lasing medium within the resonator is not exactly the same as the measured impact. The mirror separation of 50 cm meant for the mirror with radius of curvature 100 cm a confocal arrangement. The focus of the former mirror was never within the lasing medium. The considerations shown in Figures 17 and 18 apply in this part of the experiment.

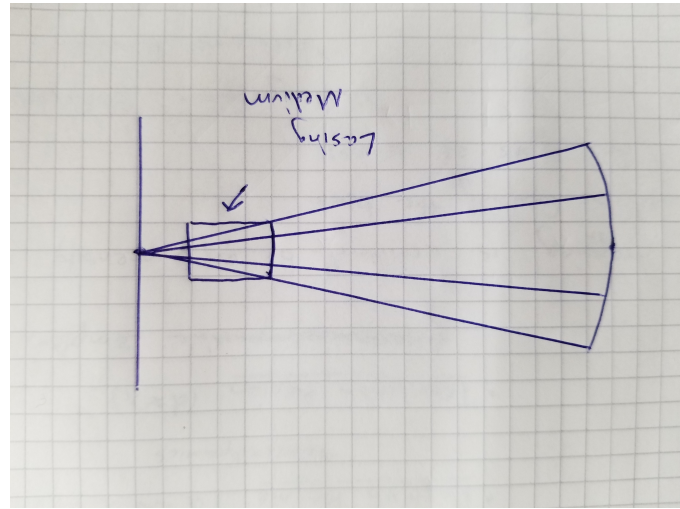


Figure 17: Interaction of Laser Beam in Optical Resonator Example 1

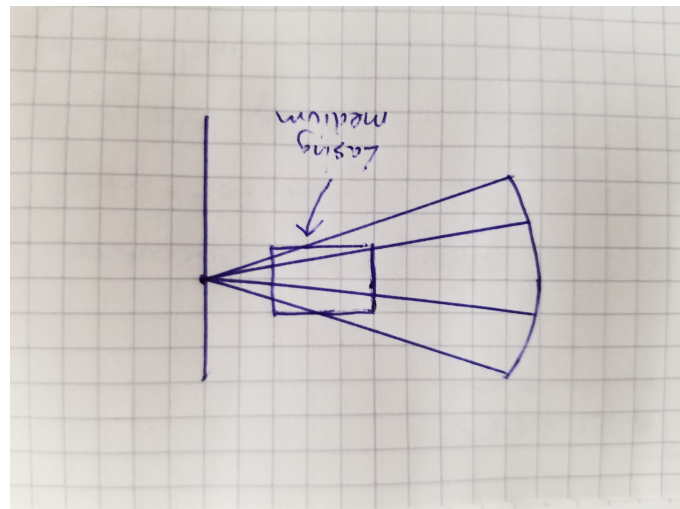


Figure 18: Interaction of Laser Beam in Optical Resonator Example 2

What is shown in the two pictures is the principle that increasing the cavity length while keeping the size of the lasing medium the same decreases the amount of light passing through the lasing medium. This less light being amplified through stimulated emission decreases the output power of the laser. Similarly, changing the position of the laser gain within such an arrangement would again change the intersection of the resonating beam with the amplifying medium. In the pictures above, moving the gain medium to the left should

increase the output power, whereas moving it to the right should decrease the output power. There is no reason to believe that this should be a linear increase, as geometrically the volume of the intersection would not increase linearly with changes in the position.

The data the group found was not consistent with these considerations. There was an optimal, centered position for the gas lasing medium, with displacements from this optimal position leading to decreases in output power. The minimum output power was experienced when the lasing medium was closest to the plane mirror, as expected.

The reasons for the discrepancy could stem from the device used. The He-Ne lasing medium seemed to have an entrance aperture on both sides. The effect of such an aperture is to block beams that hit the lasing medium outside of it. A lasing medium placed further away from the spherical mirror could actually accept larger wavefronts, and potentially more rays could be amplified and resonate, increasing the output power.

The experimental trend of output power dropping as the lasing medium was too close to either mirror could then be explained as such: when the lasing medium was too close to the spherical mirror, less light was accepted into the medium as when it was a little further away, up until the point that the He-Ne gas tube had certain parts that no longer interacted with the resonating light, nulling that volume's amplification effects. This could lead to the observed trend.

Further experiments could be made with lasing mediums of various geometries. For example, manufacturing a gas lasing medium tube with the same volume and composition of helium and neon but with a conical, tubular, and rectangular shape and placing these geometries in a variety of optical resonators with different arrangements could shed light on the aspects of the measured behavior stemming from simple geometry and areas of intersection.

#### 5.4 Determination of the Wavelength

The given laser wavelength has a value of 632.82 nanometers. The experimentally determined value was  $636.4 \pm 1.1$  nanometers. The theoretical value was not inside the bounds set by the uncertainty. The percent error is calculated as .57 percent. The reason for the discrepancy is most likely a combination of misalignment, meaning that the laser beam may not have hit the diffraction grating at perpendicular incidence, as well as the diffraction grating being perhaps bent. Perhaps most importantly, it is also important to consider the lacking uncertainty in the diffraction grating slit separation. The slit width is obviously finite, and in fact, assuming that the slits all have the exact same width, the width of one slit would need to be subtracted from the given slit spacing. It is as of right now difficult to ascertain the effect on the result – if the slit width is about .56 percent of the given slit separation however, that is, roughly 1/20 of the slit separation, then the result is in agreement with the given laser wavelength.

It is also known that most lasers don't operate at their theoretical wavelength

due to manufacturing discrepancies. The central wavelengths emitted by lasers instead lie on a type of statistical distribution around the theoretical value. It is therefore possible that the experimental value did measure the true value of wavelength.

For starters, to be able to judge, the slit width would need to be measured and the slit separation adjusted. Then, the laser wavelength could be measured using another method, perhaps with other gratings or a full-on digital spectrometer setup, and the values compared. This would shed light on the true output wavelength of the laser.

## 5.5 Laser Beam Quality Factor

Our measured value of  $M^2$  deviates largely to the ideal beam quality factor of a He-Ne laser of 1.1. This indicates bad beam quality factor of the laser generated. The high value of the beam equality factor might due to the misalignment of the cavity setup, the impurity of the environment, and the quality of the He-Ne laser tube. For ion lasers, the M2 factor is typically between 1.1 and 1.3. Collimated TEM00 diode laser beams usually have an M2 ranging from 1.1 to 1.7. (4). Compared to other types of laser, an ideal He-Ne laser has good beam quality factor that follows a Gaussian profile.

## 5.6 Suppressing the Fundamental Mode

The result that placing a string in the cavity in order to excite the first higher order TEM mode, consisting of two intensity lobes as shown in Figure 16, is expected. What was simply done is increase the cavity losses of the fundamental, symmetrical mode, which was always scattered by the string at each pass. The gain of th

# 6 Conclusion

In this experiment, we studied different properties of a gas He-Ne laser extensively. We evaluated the relation between the injection current and output power of the laser beam in terms of the voltage detected on the photo-diode of two cavities, the relation between cavity length and the output power of laser beam of two cavities, and evaluated the laser beam quality factor  $M^2$ . Due to the high sensitivity of the optimal laser output to eternal factor such as proper and accurate alignment, the influence of air dust, and the quality of the He-Ne gas tube, not all our measurement results are perfectly predicted by our mathematical models and physical models, indicating the strong uncertainty that can be generated from a gas laser. In future experiment, we may collect more data points, use a cleaner area , and improve laser cavity alignment to further and better study the different properties and characteristics of a He-Ne gas laser.

## 7 References

1. AZOptics. *Helium-Neon Lasers: Properties and Applications*. AZO Optics. <https://www.azooptics.com/Article.aspx?ArticleID=464>.
2. *He-Ne Laser*. Abbe School of Photonics. February 16, 2018.
3. *Unstable Resonator*. Encyclopedia of Laser Physics. [https://www.rp-photonics.com/unstable\\_resonators.html](https://www.rp-photonics.com/unstable_resonators.html)
4. Sciete Instruments. *M<sup>2</sup> Factor (Quality Factor)*. [http://www.scitec.uk.com/lasers/m2\\_factor.php](http://www.scitec.uk.com/lasers/m2_factor.php)